iScience

CellPress
OPEN ACCESS

Review

PbS Colloidal Quantum Dot Inks for Infrared Solar Cells

Siyu Zheng,[1] Jingxuan Chen,[1] Erik M.J. Johansson,[2] and Xiaoliang Zhang[1,*]

SUMMARY

Infrared PbS colloidal quantum dot (CQD)-based materials receive significant attention because of its unique properties. The PbS CQD ink that originates from ligand exchange of CQDs is highly potential for efficient and stable infrared CQD solar cells (CQDSCs) using low-temperature solution-phase processing. In this review, we present a comprehensive overview of CQD inks for the development of efficient infrared solar cells, which can effectively harvest the photons from the infrared wavelength region of the solar spectrum, including the importance of infrared absorbers for solar cells, the unique properties of CQDs, ligand-exchange determined CQD inks, and related photovoltaic performance of CQDSCs. Finally, we present a brief conclusion, and the possible challenges and opportunities of the CQD inks are discussed in-depth to further develop highly efficient and stable infrared solar cells.

INTRODUCTION

Infrared light absorbers that can harvest photons from the visible and infrared regions of the solar spectrum are of great importance for efficient single-junction or tandem solar cells (Lu et al., 2019). Infrared semiconducting colloidal quantum dot (CQD) received significant research interest for the application in the infrared solar cells owing to its low-cost, solution-processability, easy synthesis, and tunable infrared optoelectronic properties (Kagan et al., 2016). Compared with the conventional near-infrared light absorbers, such as silicon and GaAs that were generally prepared using costly high-temperature processing and under high-vacuum conditions, CQDs show advantages for the development of next-generation infrared solar cells (Polman et al., 2016). For instance, the bandgap energy (E_g) of CQDs can be widely adjusted by controlling the physical dimension of CQDs owing to their quantum confinement effect (Moreels et al., 2009), which shows great potential for the construction of tandem solar cells to boost the device efficiency. Meanwhile, the multiple exciton generation (MEG) that more than one electron-hole pair could be produced in the CQDs after absorbing one high-energy photon, which may provide the possibility to overcome the Shockley-Queisser limitation of a single-junction solar cell, opening a new avenue to further improve device photovoltaic performance (Semonin et al., 2011; Zhang et al., 2015). Moreover, the solution-processed CQDs make it possible to construct solar cells on the flexible substrates using solution-processing techniques, such as continuous roll-to-roll blade-coating or spray-coating method, which are very promising toward large-scale fabrication of solar cell devices (Zhang et al., 2017a, 2017b, 2017c, 2018a, 2018b, 2018c; Zhang and Johansson, 2016). In the past few years, with the fundamental investigations on the CQD surface chemistry, device physics, and device operation, impressive achievements have been obtained that both the device efficiency and stability of infrared CQD solar cells (CQDSCs) were significantly improved.

The CQD was generally synthesized using wet chemistry organometallic approaches, and the long-chain organic ligands, such as oleic acid (OA) or oleylamine (OAm), were used to cap the dot surface to stabilize the colloidal system in the solvent (Jia et al., 2019). During the construction of CQDSC devices, the long-chain insulating organic ligands need to be replaced by the short organic ligands or halide ions (Br^- or I^-) to increase electronic coupling between dots and thus lower the transport barrier of photoinduced charge carriers and passivate the surface defects to diminish charge recombination. The liquid-state ligand exchange (LSLX) strategy (also called CQD ink technologies) applied for the ligand exchange of pre-synthesized CQDs shows more advantages compared with the conventional solid-state ligand exchange (SSLX) of

[1]School of Materials Science and Engineering, Beihang University, 100191 Beijing, China

[2]Department of Chemistry-Ångström, Physical Chemistry, Uppsala University, 75120 Uppsala, Sweden

*Correspondence: xiaoliang.zhang@buaa.edu.cn

https://doi.org/10.1016/j.isci.2020.101753

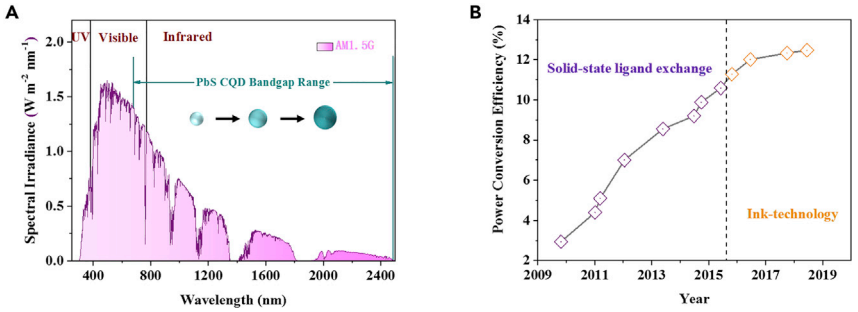

Figure 1. Solar Spectrum and PCE Evolution of CQDSCs

(A) Solar spectrum and schematic diagram of the light absorption of PbS CQDs of varying sizes.

(B) The PCE evolution of infrared CQDSCs in the past decade (from 2009 to 2019). The device efficiency was certified by NREL (https://www.nrel.gov/pv/cell-efficiency.html).

CQDs because the long-chain ligands on the dot surface could be more thoroughly replaced by the short ones, resulting in improved surface defect passivation and thus enhancing charge carrier extraction of solar cell devices (Ning et al., 2014; Liu et al., 2017). Meanwhile, the thick CQD solid films with less bandtail states could be obtained using a single-step spin-coating or blade-coating method, which shows more efficient and material usage than the conventional layer-by-layer spin-coating method (Aqoma and Jang, 2018).

To improve the infrared photovoltaic performance of CQDSCs, various metal chalcogenide CQDs were studied, including PbS (Cademartiri et al., 2006), PbSe (Zhang et al., 2017a, 2017b, 2017c), Ag_2S (Hwang et al., 2013), Ag_2Se (Tian et al., 2017), $CuInS_2$ (Peer et al., 2017), and $AgBiS_2$ (Huang et al., 2013) CQDs. Among these CQDs, PbS CQDs received more attention for the development of infrared solar cells in the wavelength region of 350–1,700 nm (E_g < 0.8 eV) and the PbS-based CQDSCs showed the highest efficiency of CQDSCs so far, which is very promising for the infrared solar cells. In this review, we provide a comprehensive summary of the progress of the PbS CQD inks for infrared solar cells. We begin with the importance of infrared absorbers for efficient infrared solar cells and the state-of-the-art infrared CQDSCs. Then, the unique properties of CQDs, such as tunable infrared E_g and solution-processable, are introduced to highlight the advantages of CQDs for infrared solar cells. After that, the fundamental breakthroughs in the CQD inks are summarized, and the optoelectronic properties of the CQD solid films affected by the ink technologies are discussed in-depth. Meanwhile, the photovoltaic performance of infrared CQDSCs fabricated with the CQD inks is demonstrated. Finally, the conclusions are presented, and the possible challenges and opportunities of CQD inks are discussed to shine the light on further developing highly efficient and stable infrared solar cells.

SOLAR SPECTRUM AND STATE-OF-THE-ART CQDSCS

The efficient usage of solar energy from the infrared region is critical for infrared solar cells. Figure 1A shows the energy distribution of solar energy with the AM1.5G spectrum. It can be seen that ~46% of the total solar energy distributes in the visible wavelength region, and ~5% and ~49% of the solar energy are from UV and infrared wavelength regions, respectively. Therefore, efficient utilization of infrared energy could open a feasible way to improve the photovoltaic performance of solar cells. The light absorption spectrum of some photovoltaic materials, such as metal halide perovskites and organic light absorbers, generally locates in the visible wavelength region, which may hinder further improving utilization of the solar spectrum. PbS CQDs possess a wide light absorption spectrum and the E_g can be finely tuned in a range of 0.8–1.6 eV by controlling the dot size that the dot with a bigger size has a lower E_g (Chan et al., 2017). Such a wide light absorption spectrum of CQDs is highly potential for infrared solar cells. The infrared solar cell is also very promising to be used as a sub-cell to combine with other cells with different light absorption wavelength for the construction of tandem or multiple junction solar cells, which could extend the light absorption range of solar cells to the infrared wavelength region. It is worthy to note that the PbS CQDSCs with a E_g of 1.3–1.4 eV (Shockley and Queisser, 1961) gave the highest efficiency of above 13% because the CQDSC is a complex system and the surface properties of CQDs and device physics of solar cells need to be finely controlled (Sun et al., 2020).

In the past few years, significant progress was obtained in the infrared CQDSCs through breakthroughs on the surface chemistry of CQDs, device physics, and device structure optimization of solar cells.

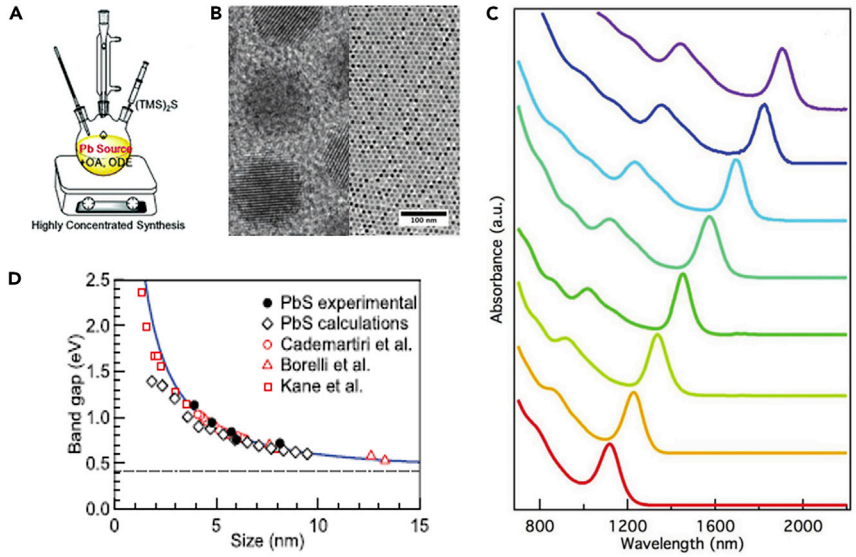

Figure 2. Infrared CQDs and Optical Properties

(A) Schematically presents the synthesis of CQDs. Adapted with permission from Zhou et al. (2019). Copyright (2019) The Royal Society of Chemistry.

(B) TEM images of CQDs.

(C) Light absorption spectra of CQDs with different dot sizes. Adapted with permission from Xia et al. (2019). Copyright (2019) WILEY-VCH Verlag GmbH & Co. KGaA, Weinheim.

(D) Relationship between the E_g and the dot size of CQDs. Adapted with permission from Moreels et al. (2009). Copyright (2009) American Chemical Society.

Subsequently, the power conversion efficiency (PCE) of infrared CQDSCs was increased from ~3% in 2010 (Luther et al., 2010) to a recent over 13% (Choi et al., 2020a, 2020b), and the device stability was also largely improved. Figure 1B presents the PCE evolution of CQDSCs with the years. In the period of 2009–2016, the efficient CQDSCs were generally fabricated using the SSLX method with layer-by-layer deposition of CQD solid films. After that period, the CQD inks appeared that the CQD solid films could be deposited using concentrated CQD inks, which was prepared using the LSLX method of CQDs. The CQD ink technologies could more thoroughly remove the long-chain insulating ligands on the CQD surface and thus efficiently passivate the surface defects of CQDs, therefore leading to improved optoelectronic properties of CQD solid films and photovoltaic performance of solar cell devices (Zhang et al., 2019). The CQD inks also provide a possibility for large-scale fabrication of the solar cells using solution-processed approaches, such as continuous roll-to-roll blade-coating, spray-coating, or print-coating methods. Therefore, the CQD inks show high potential for infrared solar cells.

INFRARED PBS CQDS

The unique physical and chemical properties of PbS CQDs are attributed to their quantum effects that when the dimensional size of semiconducting materials reaches the nano-size the size confinement will cause quantum confinement effects, exhibiting interesting physical and chemical properties that are significantly different from macroscopic materials. In this section, we discuss the recent advances of the well-developed PbS CQDs for the application in infrared solar cells.

Synthesis and Optical Properties of PbS CQDs

The conventional PbS CQDs were generally synthesized using solution-based organometallic route techniques, called the hot-injection method, and subsequently the CQDs capped with the long-chain OA ligands were stabilized in the solvent forming a colloidal system (Sargent, 2012). As shown in Figure 2A, during the preparation of CQDs, the lead (II) oxide (PbO) and oleic acid (OA) are usually used as the lead source and surface ligands, respectively, and under the high temperature and inert condition the lead oleate is formed. The bis(trimethylsilyl) sulfide [$(TMS)_2S$] is applied as the sulfur source that the $(TMS)_2S$ solved in the 1-octadecene (ODE) is quickly injected into the lead oleate solution and the colorless lead oleate solution quickly changes into a dark color, which suggests that the CQDs are nucleated and grown

in the solution (Hines and Scholes, 2003). By controlling the reaction conditions, such as precursor concertation, injection temperature of $(TMS)_2S$, and reaction time, the dimensional size and shape of CQDs can be well adjusted in a relatively easy way, thereby allowing one to control the E_g of CQDs (Hou et al., 2016).

Voznyy et al. (2019) applied a machine learning method to identify the available experimental conditions for the synthesis of PbS CQDs and established a continuous numerical model of the parameter space. Finally, the recorded parameter range to prepare the monodisperse CQDs was obtained. Other synthetic methods, such as biomineralization (Spangler et al., 2016) and ion exchange, were also studied for the synthesis of CQDs. Xia et al. (2019) demonstrated that the CQDs could be synthesized from ZnS nanorods using a cation exchange approach and the resulted CQDs had a low infrared E_g. Zhang et al. (2017a, 2017b, 2017c) prepared the CQDs using the cation exchange of CdS CQDs and Ostwald ripening that the synthesized CQDs presented extremely narrow size distribution, good surface passivation, and air stability. The transmission electron microscope (TEM) image of the CQDs synthesized using the cation exchange method is shown in Figure 2B. Moreover, the CQDs showed strong light absorption covering the visible and near-infrared wavelength regions, and the light absorption spectrum can be well adjusted in the infrared region by controlling the dot size. The CQDs with a larger size had a wider light absorption spectrum with lower E_g (Figure 2C), which is of great importance for the construction of multi-junction solar cells to selectively harvest photons from the solar spectrum. Based on the previous studies, Moreels et al. (2009) figured out the relationship between the size of CQDs and E_g (Figure 2D) that the size depended E_g of CQDs can be expressed using the equation

$$E_g = 0.41 + \frac{1}{0.0252d^2 + 0.283d} \quad \text{(Equation 1)}$$

where E_g and d are the bandgap energy and diameter of PbS CQDs, respectively. With such an equation, the size of CQDs can be easily calculated from the E_g, which could be obtained from the light absorption spectrum, avoiding using complex TEM analysis of each synthesized CQDs.

These unique properties of CQDs have promoted the development of infrared CQDSCs. The tunable E_g of CQDs enables them to harvest photons from the infrared wavelength region that could not be absorbed by other photovoltaic materials, such as perovskite materials and organic photovoltaic materials.

Solution-Processability of CQDs

Another important advantage of CQDs for infrared solar cells is solution processability because the CQD was generally synthesized in a liquid state. Therefore, various solution-processed techniques, such as spin-coating, spray-coating, printing, or ink-jet printing method, can be applied for the deposition of CQD solid films (Figure 3A). The solution processability of CQDs allows fabrication of the solar cells on the flexible substrates under low temperature toward scalable and low-cost manufacture. Especially, the CQD inks prepared using the LSLX method further promoted the fabrication techniques that a thick CQD solid film could be prepared using a single-step deposition method under low temperature. In this section, we summarize the recent advances in the fabrication methods of solar cells using the solution-processed strategies.

So far, most of the highly efficient infrared CQDSCs were fabricated using the spin-coating method for laboratory studies (Figure 3B; Fischer et al., 2013). However, such a fabrication approach has a limitation on the size of substrates and it is significantly challenging to achieve large-scale production of solar cell devices. Meanwhile, the usage efficiency of CQDs is low using the spin-coating method to fabricate solar cells. With the continuous development of CQDSCs, the scale-fabrication with high material usage of CQDs is significantly required toward the commercial applications. Therefore, more attention was put on the scalable deposition of high-quality CQD solid films using novel solution-processed techniques with CQD inks.

Most of the efficient CQDSCs were constructed by stacking the n-type CQD solid film treated with halide ions (I^- and Br^-) with the p-type CQD solid film treated with 1,2-ethanedithiol (EDT). The p-type CQD solid film was usually prepared using the spin-coating method with the SSLX process of CQDs (Wang et al., 2018). To develop the SSLX free solar cell devices, Aqoma et al. (Aqoma and Jang, 2018) prepared the p-type and n-type CQD inks to fabricate the CQDSCs using a blade-coating technique, which could deposit uniform CQD solid films for a large scale and increase the material usage efficiency of CQDs. Finally, the infrared CQDSCs fabricated with a blade-coating technique had a PCE of over 10%. Furthermore, the CQDSC devices were allowed to be constructed on the flexible substrates using such CQD inks, which

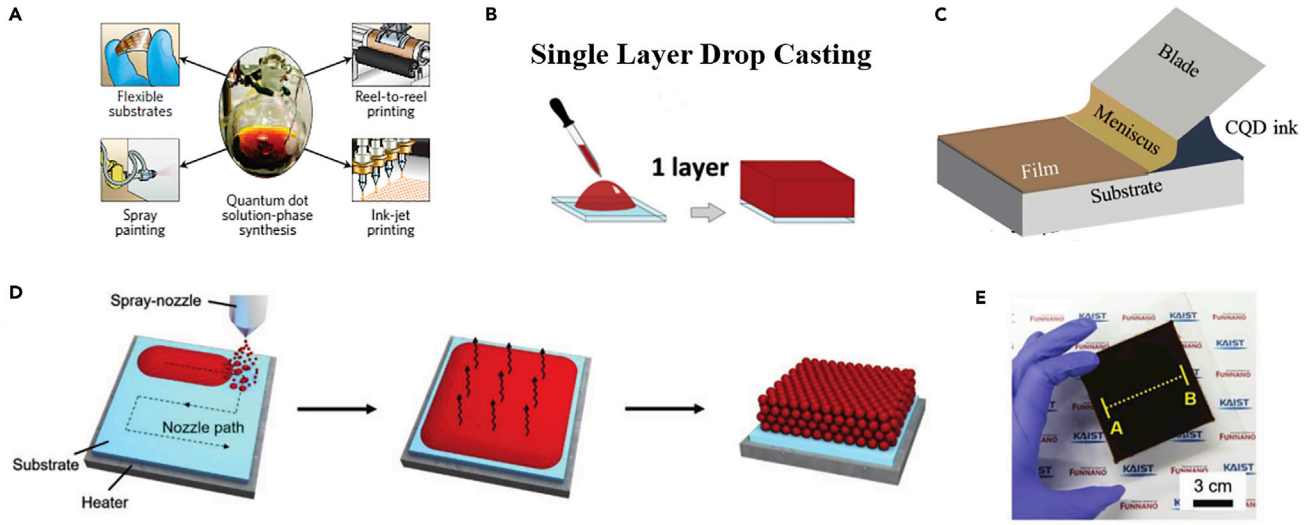

Figure 3. Solution-Processability of Infrared CQDs

(A) Picture of CQD solution and different solution-processed techniques, such as spin-coating, spray-coating, reel-to-reel printing, and ink-jet printing, can be applied for the deposition of CQD solid films. Adapted with permission from Sargent (2012). Copyright (2012) Springer Nature.

(B) Schematic of single layer drop-casting process. Adapted with permission from Fischer et al. (2013). Copyright (2013) WILEY-VCH Verlag GmbH & Co. KGaA, Weinheim.

(C) Schematic of blade-coating process of CQD solid films. Adapted with permission from Kirmani et al. (2018). Copyright (2018) WILEY-VCH Verlag GmbH & Co. KGaA, Weinheim.

(D) Scheme of the deposition process of CQD solid films using the spray-coating method.

(E) Photograph of the CQD solid film prepared on a large substrate (10 × 10 cm^2). Adapted with permission from Choi et al. (2019). Copyright (2019) WILEY-VCH Verlag GmbH & Co. KGaA, Weinheim.

provided a big step toward the scalable fabrication of CQDSCs (Figure 3C). Kramer et al. (2014) demonstrated that the CQDSCs with a relatively low efficiency fabricated using the blade-coating method under high humidity conditions could be turned into stable and efficient CQDSCs by placing the devices in a dry environment for a short time. These important studies may overcome the challenges of scalability fabrication and device stability of CQDSCs.

In addition to the scalable blade-coating method, the spray-coating method also enabled fabrication of CQDSCs on the flexible substrates (Figure 3D). The spray-coating technique provided a feasible method to deposit uniform CQD solid films with continuous roll-to-roll production. Meanwhile, by using the spray-coating method, the CQD solid films can be deposited on the unconventionally shaped substrates, such as curve substrates, which are adaptable for various practical applications. Kramer et al. (2015) explored the versatility of the spray-coating technique by fabricating the CQDSCs on different substrates and further tested the manufacturability of such a process on flexible substrates. Choi et al. (2019) studied the kinetics of the solute redistribution during the spray-coating process and prepared a large area uniform CQD solid film by adjusting the solvent evaporation rate (Figure 3E).

The development of various solution-processed methods for the fabrication of CQDSCs is conducive for commercialization, which may not require the costly high vacuum or temperature types of equipment. From the initial spin-coating method to the appearance of blade-coating or spray-coating techniques, the CQDSCs were developed to also work in large-scale industrial production instead of only being studied in laboratory research. The development of these technologies laid the foundation for the roll-to-roll continuous manufacturing process of CQD inks in the future. Currently, Jang et al. (2015) had successfully achieved roll-to-roll CQDSC manufacturing on the flexible substrates with the SSLX method. Bar coater was applied with micro-patterns on the surface to realize the stripe patterning of CQD solid films, and the subsequent solution dipping completed the ligand exchange. Screen printing of silver paste electrodes that replaced the complicated vacuum evaporation further promotes large-scale roll-to-roll manufacturing. Moreover, they pointed out that the CQD inks that do not require ligand exchange can also be implemented in this roll-to-roll process. However, the device photovoltaic performance of the solar cells

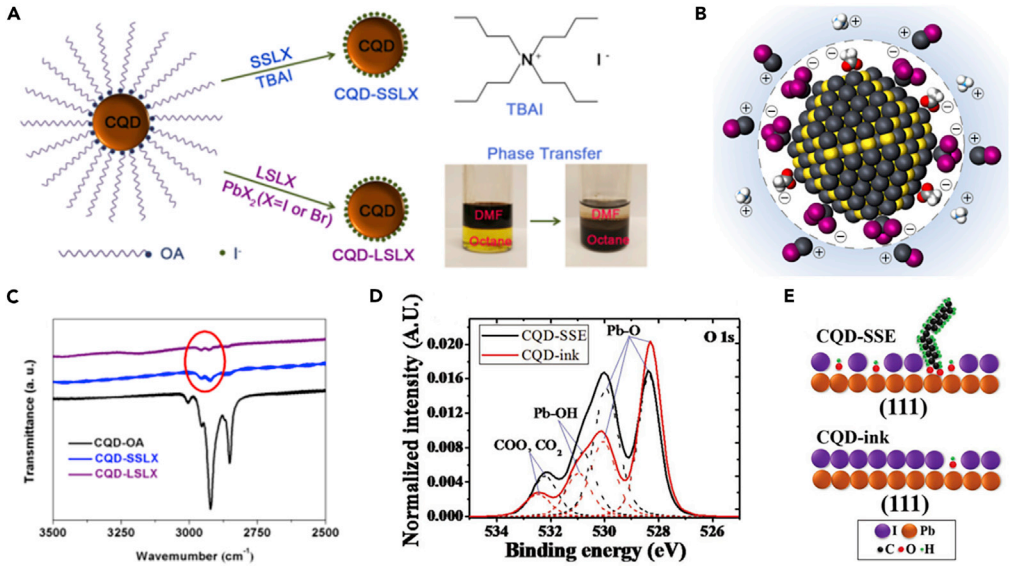

Figure 4. Ligand Exchange of CQDs

(A) Schematic illustration of the ligand exchange using SSLX and LSLX approaches. Adapted with permission from Zhang et al. (2019). Copyright (2019) American Chemical Society.

(B) Schematic illustration of the CQD surface. The dot surface was stabilized by both PbX^+ and NH_4^+. Adapted with permission from Liu et al. (2017). Copyright (2017) Springer Nature.

(C) FTIR spectra of the CQD-SSLX and CQD-LSLX solid films. Adapted with permission from Zhang et al. (2019). Copyright (2019) American Chemical Society.

(D) XPS signal from O 1s of iodide-passivated CQD layers (dotted lines are the deconvoluted peaks).

(E) Surface illustrations of the {111} facets of iodide-passivated CQDs. Adapted with permission from Aqoma et al. (2017a, 2017b). Copyright (2017) WILEY-VCH Verlag GmbH & Co. KGaA, Weinheim.

fabricated with blade-coating or spray-coating techniques was still lower than that of the solar cells fabricated with the conventional spin-coating method, which suggested that more fundamental studies needed to be conducted to improve the optoelectronic properties of the CQD solid films prepared using the novel blade-coating or spray-coating techniques.

PBS CQD INKS

CQD inks originated from the LSLX of CQDs. Compared with the SSLX of CQDs, the CQD inks provide a more efficient way to thoroughly remove the long-chain surface ligands of CQDs. Meanwhile, the CQD solid films could be prepared using a single-step deposition process of CQD inks, showing potential for large-scale production of infrared solar cells. In this section, we will comprehensively discuss the recent advances of CQD inks and applications in infrared solar cells.

Ligand Exchange of PbS CQDs

As demonstrated above, the PbS CQDs were synthesized in the solution phase and the dot surface was capped with long insulating ligands, such as OA, which need to be replaced with short ones to enhance the carrier mobility in the CQD solids as fabricating the optoelectronic devices (Ning et al., 2014). Meanwhile, the surface defect passivation of CQDs is critical to lower the charge recombination in the solar cells, thereby improving device photovoltaic performance. Both SSLX and LSLX methods could remove the surface long-chain ligands of CQDs. Zhang et al. (2019) comprehensively studied the effect of SSLX and LSLX methods on the optoelectronic properties of CQD solid films and the photovoltaic performance of infrared CQDSCs, as shown in Figure 4A. The layer-by-layer (LBL) deposition approach was generally combined with the SSLX of CQDs to prepare CQD solid films for CQDSCs. Briefly, the CQDs capped with long-chain OA ligands was spin-coated on the substrates and subsequently the short-ligand solution, such as tetrabutylammonium iodide (TBAI) (Lu et al., 2018), 1-ethyl-3-methylimidazolium iodide (EMII) (Stavrinadis et al., 2017), or 3-mercaptopropionic acid (MPA) (Bi et al., 2018a, 2018b), was applied to soak the CQD solid films for the ligand exchange. It is worthy to note that the surface ligands of CQDs may not be thoroughly

replaced by the short ones, which suggests that the surface defects of CQDs could not be efficiently passivated using the SSLX method for the deposition of CQD solid films.

To solve such issues, the LSLX method of CQDs was further developed that the ligand exchange was carried out in the solution with a phase transfer, and finally, the concentrated CQD ink was obtained with short ligands capping on the CQD surface. Significant progress of the CQD inks was obtained in the past few years, especially the CQD inks for the infrared photovoltaic (Ning et al., 2014) and photodetector devices (Sliz et al., 2019). During the preparation of CQD inks, the lead halide, such as PbI_2 and $PbBr_2$, was used as ligands to replace the OA ligands on the dot surface. As shown in Figure 4A, dimethylformamide (DMF) that dissolved PbX_2 (X = I and Br) was added into the OA-capped CQD octane solution. After stirring the mixed solution the CQDs transferred from the non-polar phase (octane) to the polar phase (DMF) to produce halide-capped CQDs. Since a double layer of PbX_3^-, NH_4^+, and PbX^+ was formed on the dot surface, the CQDs could uniformly disperse in the polar DMF solvent and maintain the colloidal system (Figure 4B). Finally, the CQD powder was collected and dispersed in the polar solvents, such as DMF, chlorobenzene, and butylamine (BTA), forming CQD inks.

Direct synthesis of CQD inks was reported recently, which could simplify the preparation of CQD inks. Wang et al. (2019) used PbI_2 and diphenylthiourea (DPhTA) as the lead source and sulfur source, respectively, accompanied by the injection of BTA into the reaction system. Alkaline conditions promoted the conversion of DPhTA to SH to react with PbI_2 to obtain PbS CQDs capped with I^- ligands, while the BTA can control the nucleation and growth of CQDs, finally achieving uniform-sized CQDs. This novel room temperature synthesis method could substitute the traditional cumbersome ligand exchange steps, thereby realizing large-scale and low-cost manufacture for CQDSCs. This method provided a new avenue and commercialization prospect for the development of CQD inks and solar cells.

The high-quality CQD solid films can be achieved using a single-step spin-coating or blade-coating deposition method toward the scalable preparation of CQD sold films. Figure 4C shows the Fourier transform infrared (FTIR) spectra of CQD solid films that the peaks at 2,855, 2,914, and 2,955 cm^{-1} were corresponding to the C-H stretching of OA ligands (Zhang et al., 2019). Most of the OA ligands were removed during the SSLX or LSLX process, whereas the removal of OA ligands using the LSLX method was more complete. Figure 4D shows the X-ray photoelectron spectroscopy (XPS) spectra of O 1s of the CQD-SSLX and CQD-LSLX films, indicating that the intensity of Pb-OH and -COO, CO_2 is much lower in the CQD-LSLX film (Aqoma et al., 2017a, 2017b). These important results reveal that the OA ligands on the dot surface could be more thoroughly replaced using the LSLX method and obtain improved surface defect passivation of CQDs (Figure 4E). Compared with the SSLX method, the LSLX method for the deposition of CQD solid films could enhance CQD coupling and promote carrier transport between CQDs. Furthermore, the improved surface defect passivation of CQDs could inhibit generation of sub-bandgap trap states, increasing the charge extraction of CQDSCs. Therefore, the CQDSCs fabricated with the LSLX method had higher efficiency compared with that of the devices fabricated with the conventional SSLX method, and the state-of-the-art CQDSCs were fabricated using the LSLX method so far.

The stability of the CQD ink is of great importance for studies and industrial applications. The surface ligands of CQDs were usually unstable in the polar solvent, which could lead to aggregation or degradation of CQDs. Compared with the CQDSCs fabricated with the fresh CQD inks, the device efficiency of the CQDSCs fabricated with the aged CQD inks significantly dropped, which suggests that the CQD inks could not maintain long-term storage. Gu et al. (2019) added MPA into the CQD inks to replace the -OH group, and the results showed that the thiol (-SH) groups and part of carboxyl (-COOH) groups could replace -OH groups to chemically bond on the dot surface. Moreover, MPA also improved the stability of CQD inks. The -COOH groups in MPA had a strong interaction with BTA, which increased the dispersibility of CQDs and thus ensured the ink stability. The results indicate that the CQD ink treated with MPA did not aggregate for at least 50 days and the CQDSCs prepared with the ink aged for 1 day also gave high efficiency.

However, the large-sized infrared CQDs with a low E_g was not suitable for the conventional LSLX method. Kim et al. (2019) reported that the CQDs with a low E_g exposed more non-polar {100} facets, which could not be efficiently passivated by lead halide. Therefore, the CQDs were aggregated or even fused during the ligand exchange since the OA ligands on the {100} facet of CQDs were easily removed in polar solvents, such as DMF. The NaAc instead of ammonium acetate (AA) was applied in the LSLX and the Na^+ was

preferentially combined with the {100} facets of CQDs and had a higher adsorption strength than that of NH_4^+, suppressing the fusion of the {100} facets of CQDs and also leading to improved surface passivation. Therefore, the surface chemistry of the CQDs with a low E_g is somewhat different from that of the high E_g CQDs, thereby the existing conventional LSLX and ink preparation processes maybe not meet the needs of the CQDs with a low E_g ($Eg < 1$ eV). Further studies need to be carried out on the surface chemistry of the CQDs with a low E_g.

The research of CQD ink has laid a strong platform for infrared solar cells. Since Liu et al. developed the AA-assisted lead halide LSLX method, CQD ink has gradually replaced the SSLX method for device construction. The stable CQD ink with less surface defect of CQDs has led to breakthroughs in device photovoltaic performance, and a simple manufacturing process significantly promoted the improvement of device architecture and commercialization of CQDSC devices. However, there are still challenges in the ink stability of small bandgap CQDs. Owing to their different surface properties, the effective passivation method of small bandgap CQDs still needs further exploration, thereby realizing the application of small bandgap CQDs in single-junction and multi-junction solar cells.

Solvent Engineering of CQD Inks

The solvent of CQD inks significantly affects the quality of CQD solid films and therefore determines the photovoltaic performance of CQDSC devices. As to prepare a thick CQD solid film using the single-step deposition process, the CQDs should be precipitated from the DMF solvent during the ligand exchange and subsequently redispersed in a quick-drying solvent forming a concentrated CQD ink. So far, the general solvent used for the CQD inks was BTA. However, the BTA solvent processes a high polarity that could dissolve CQDs and thus affect the ink stability (Jia et al., 2019). Therefore, different solvents were studied to meet the requirements of CQD inks under different conditions.

Solvent engineering provides a feasible way to promote the uniform distribution of the matrix in the CQD solid films, thereby improving device performance. Xu et al. (2018) replaced the BTA solvent with a hybrid amine (BTA, amylamine and hexylamine) solvent. The coordination complex of the hybrid amine and the lead halide resulted in the formation of a two-dimensional (2D) restricted PbI_2 matrix, which could uniformly space CQDs in the CQD solid films (Figure 5A). The inhomogeneity of the 3D free growth matrix generally led to excessive isolation and/or surface fusion of CQDs, whereas the 2D PbI_2 matrix could reduce the structural and energy disturbances of CQD solid films (Figure 5B). Excessive isolation of CQDs in the CQD solid films hindered the charge carrier transport and excessive CQD coupling could also increase the open-circuit voltage (V_{OC}) losses. The uniform matrix addressed these issues that the 2D matrix improved the carrier transport between dots and thus increased the charge carrier diffusion length in the CQD solid films, which generally limited the thickness of the CQD solid photoactive layers in the solar cells. Therefore, with the application of a hybrid amine solvent, the CQDSCs with almost twice the thickness of the photoactive layer was fabricated, thereby simultaneously increasing device V_{OC} and short circuit current density (J_{SC}), and an efficiency of over 12% was obtained.

Solvent engineering also motivated the development of low E_g CQDs for infrared solar cells. Figure 5E (Kiani et al., 2016) demonstrated that using BTA as a solvent for the CQDs with a low E_g of 1 eV resulted in the mass agglomeration of CQDs. Therefore, a mixed solvent of hexylamine (HXA) and butanone (MEK) (HAX:MEK = 20:80%) was used instead of the BTA solvent, wherein, HAX could completely disperse CQDs and MEK provided a low boiling point. Such a mixed solvent can be applied to prepare the CQD inks with a concentration of ~200 mg/mL, which provided a sufficient concentration of CQD inks for the deposition of CQD solid films with enough thickness and low roughness (Figures 5C and 5D). Meanwhile, the changes in the spectra of CQDs dispersed in different solvents were neglectable and the Stokes shift in the spectra was also comparable with the previous studies, which indicated that the changes in the solvent did not affect the physical properties of CQDs. This study largely improved the stability of CQD inks and the quality of CQD solid films for the low E_g CQDs. It is notable that for CQDs with a low E_g, solvent engineering was very important to improve the stability of CQD inks, which was a research direction for the development of infrared solar cells.

Solvent engineering of CQD inks also provides the possibility for the construction of grading structured CQDSCs. Since the polar BTA solvent will re-disperse and destroy the underlying CQD solid films, fabricating graded CQDSCs using the LSLX method remains a challenge. Kim et al. (2018a, 2018b) solved

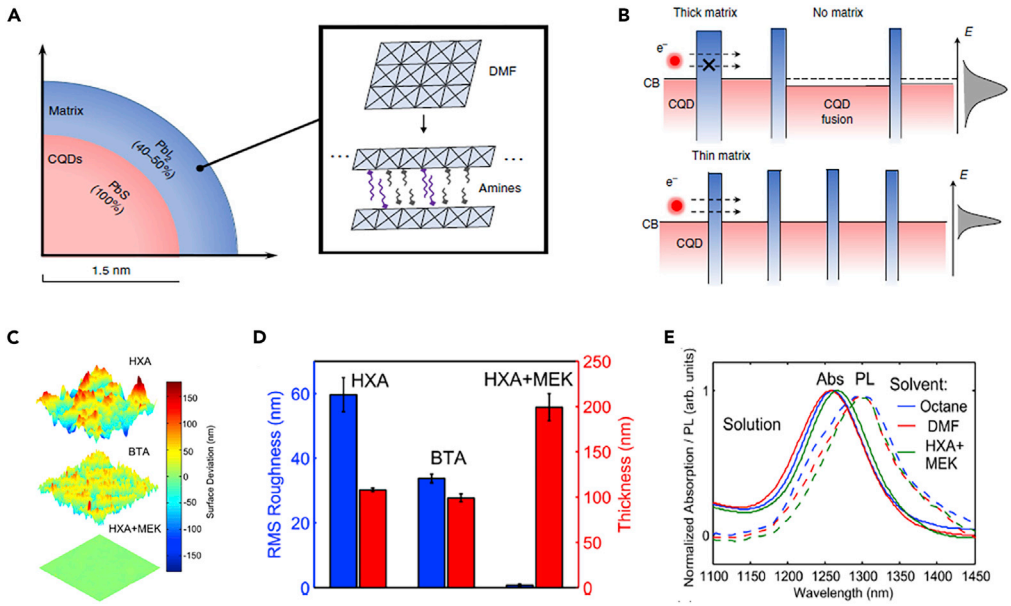

Figure 5. Solvent Engineering of CQD Inks

(A) The structure of the CQD surface passivated with a 2D layered structure.

(B) Schematic diagram of the relationship between the photocarrier transport between CQDs and the thickness of the gap matrix on the atomic scale. Adapted with permission from Xu et al. (2018). Copyright (2018) Springer Nature.

(C) The AFM surface topology of CQD solid films processed from HXA, BTA, and HXA + MEK.

(D) Roughness and thickness of CQD solid films.

(E) Normalized absorption (solid line) and PL (dashed line) spectra of CQDs in the solution. Adapted with permission from Kiani et al. (2016). Copyright (2016) AIP Publishing.

this issue by using non-polar CQD inks that the BTA was introduced as a phase transfer catalyst to dissolve CQDs forming CQD-BTA complexes. The lone pair of electrons of the primary amine group and the -C-H alkyl chain could promote the interaction between the polar surface of CQDs and the non-polar solvent, and subsequently the CQDs were dispersed very well in the non-polar solvent. Moreover, the low boiling point of BTA ensured that the BTA was easily removed by the subsequent thermal annealing process. The graded structure of the CQD layers with a high E_g CQD solid layer on the top of the low E_g CQD solid layer facilitated band alignment within the solar cells. Since a widened depletion junction was formed at the back of the device, the charge extraction was significantly improved and the device gave an efficiency of up to 12.3%.

The polarity and volatility of CQD ink solvents are criteria for the quality of CQD solid films. The high-polarity solvent could promote the dissolution of CQDs and underlying films, which is not conducive to ink stability. The highly volatile solvents are beneficial to improve the flatness of CQD solid films. For solvent engineering, finding a polar solvent suitable for CQDs with different bandgaps is the key direction. Therefore, through the solvent engineering of CQD inks, the optimization of CQD solid films and CQDSC devices can be achieved. Although BTA was widely used as the solvent in the CQD inks, solvent engineering is still needed to be further studied to dissolve large-sized CQDs toward the development of infrared solar cells with a broad light-harvesting spectrum. Furthermore, solvent engineering is one of the most important strategies to prevent the disorder of energy and structure in the CQD solid films and thus results in the improved photovoltaic performance of devices.

Surface Chemistry of PbS CQDs

CQD has a large specific surface area that significantly affects the optoelectronic properties of CQD solid films, therefore directly determining the photovoltaic performance of CQDSCs. The synthesized PbS CQDs are mainly composed of lead-rich {111} facets, which are accompanied by capping OA and OH ligands. Generally, for solar cell applications, these original ligands need to be thoroughly removed to reduce trap states and improve conductivity of CQD solid films (Xia et al., 2020). The surface chemistry of CQDs

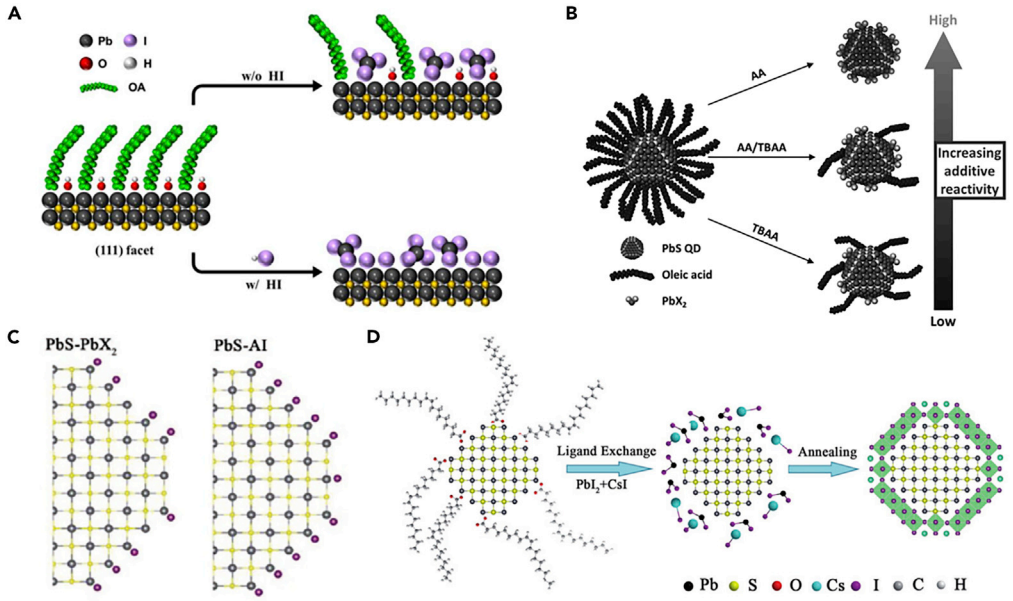

Figure 6. Surface Chemistry of CQDs

(A) Schematic illustration of HI-assisted solution-phase ligand exchange on the {111} facets of CQDs. Adapted with permission from Jo et al. (2018). Copyright (2018) American Chemical Society.

(B) Schematic illustration of the reactivity control during solution-phase ligand exchange of CQDs by mixing AA and TBAA reagents. Adapted with permission from Jo et al. (2017). Copyright (2017) WILEY-VCH Verlag GmbH & Co. KGaA.

(C) Schematic illustration of the surface passivation of PbS-PbX_2 and PbS-AI QD. Adapted with permission from Jia et al. (2019). Copyright (2019) WILEY-VCH Verlag GmbH & Co. KGaA.

(D) Schematic illustration of the fabrication process of inorganic $CsPbI_3$ perovskite coating on the CQDs. Adapted with permission from Zhang et al. (2018a, 2018b, 2018c). Copyright (2017) WILEY-VCH Verlag GmbH & Co. KGaA.

is dedicated to replacing the original long-chain ligand with short ones, and the resulting physical and chemical properties of CQDs are significantly affected by these short ligands. For CQD inks, the CQD surface is modified by halide ions after the phase transfer process, which finally forms a stable ink in a polar solvent under a combination of PbX^+ and PbX_3^- on dot surface. Meanwhile, the stability of CQD inks is also affected by the surface chemistry of CQDs. The solvent polarity significantly affects the stability of ligands, especially on the {100} facets with a low binding force of OA. The exposed surface of CQDs with high surface energy generally results in an agglomeration of CQDs. Therefore, surface chemistry is vital for the studies of CQD inks and the performance of solar cells. Extensive studies on the surface chemistry of CQDs were carried out, and most of them were dedicated to improve the surface passivation of CQDs and suppress energy disorder in the CQD solid films. In terms of CQD inks, the surface chemistry of CQDs includes additive engineering and ligand engineering. Herein, we comprehensively discussed the surface chemistry of CQDs for the CQD inks.

As the above description, lead halide (PbI_2 and $PbBr_2$) was widely applied as ligands in LSLX for the preparation of CQD inks. By adding additives to such LSLX, further promoting the surface defect passivation of CQDs and adapting to different requirements can be realized. Jo et al. (2018) found that using HI as an additive can provide both dense packing and surface passivation of CQDs (Figure 6A). Hydrogenated acid helped to remove the OA ligands that remained on the CQD surface, which contributed to the deposition of dense CQD solid films. Meanwhile, I^- could replace the -OH groups on the CQD surface, providing extra passivation and inhibiting CQD fusion. Liu et al. (2019a, 2019b) used formic acid (HCOOH) to control steric hindrance and promote the ligand exchange process. This work showed that the coverage of OA on the surface of large-sized CQDs was ~80%, which resulted in a large steric hindrance and prevented the diffusion of lead halide ligands. HCOOH could diffuse between OA ligands and attach to the OA vacancy on the PbS{111} facets with stronger binding energy and thus increased the packing density of ligands. Owing to the steric effects of ligands, OA ligands were forced to rearrange on the dot surface that ultimately weakened the binding energy of OA ligands. As a result, lead halide ligands could more completely replace OA

ligands and thus improved surface defect passivation and energy uniformity of CQDs. The above studies suggest that the insufficient ligand exchange may occur for the CQDs with a low E_g and the additives may be needed to promote the ligand exchange and surface defect passivation.

Choi et al. (2020a, 2020b) prepared a shielding layer on the CQD surface by introducing KI into the ligand exchange process. For the passivation of CQD with PbI_2 and KI, KI buffer layer protected the underlying S site from O_2, thereby preventing the oxidation of CQDs. Devices with KI buffer layer aged for 50 h under continuous air operation did not show obvious degradation in PCE and maintained 80% of the initial efficiency after illumination for 300 h. It can be seen that the main purpose of the additive engineering is to enhance the surface passivation of CQDs and thus reduce long alkyl ligand residues. However, Jo et al. (2017) reported that keeping trace OA on the CQD surface contributed to the improvement of device V_{OC}. The weak acidity of tetrabutylammonium iodide (TBAA) benefited to retain OA ligands, which inhibited fusion and etching between CQDs (Figure 6B). The enhanced monodispersity of CQDs suppressed energy disturbance and a bandtail state, thereby reducing the energy loss in devices. Although the retention of OA resulted in a decrease in carrier mobility and an increase in radiation recombination loss, fine controlling the proportion of TBAA (AA:TBAA = 0.2:0.8) could avoid the significant decrease in device J_{SC} and fill factor (FF) and the device efficiency was eventually improved from 10.1% to 10.9%. These studies confirmed that additive engineering could effectively control the ligand exchange process, thereby tuning the surface chemistry of CQDs.

Currently, most efficient CQDSCs were fabricated using inorganic halide ligands to passivate CQD surface. Ning et al. (2014) proposed photovoltaic-quality n-type CQD inks for the first time. The cation was dissolved in BTA solvent and the CQD with I^- on the CQD surface resulted in electrostatic repulsion between CQDs, thereby stabilizing CQDs in solution. Liu et al. (2017) and Aqoma et al. (2017a, 2017b) demonstrated that the CQDSCs with lead halide applied as ligands achieved an efficiency of over 11%. Sun et al. (2017) used pseudohalide thiocyanate anion (SCN^-) together with PbI_2 as a passivating agent to achieve hybrid surface passivation. Quasi-halogen was polyatomic analogs of halogens, whose chemical properties allowed them to replace halogen atoms through strong chemical interactions with the CQD surface. Figure 6C (Jia et al., 2019 used NH_4I instead of lead halide as surface ligands for the LSLX process. Compared with lead halide ligands, NH_4I could more thoroughly replace OA ligands on the CQD surface, reducing carrier recombination caused by trap states (Han, 2020). For the large-sized CQDs, more charge-neutral PbS {100} facets hindered effective surface passivation, thus the CQD surface tended to oxidization and fusion. PbI_2 passivation could not cover the entire surface. The CQDs passivated by $PbCl_2$ exhibited better passivation, but thick $PbCl_2$ shell led to poor charge transport within CQD solid films. The CQDs passivated by $PbBr_2$ had higher charge mobility, but the passivation was worse. Mixed lead halide ligands could combine the advantages of these three ligands and each lead halide could be exchanged to its most energy-supported surface, improving passivation and carrier transport (Fan et al., 2019). Therefore, the superior surface passivation of CQDs could improve device performance and also promotes ink stabilization.

Metal halide perovskite and CQD have good lattice matching, so the perovskite can epitaxially grow on the CQD surface forming a coating layer. For perovskite-coated PbS CQDs, the lattice anchoring between the two materials could achieve mutual reinforcement (Liu et al., 2019a, 2019b). Owing to the fixation of CQDs, the crystal transformation of perovskite was suppressed, thus maintaining excellent air stability. Furthermore, the perovskite coating could protect CQDs from oxidation and agglomeration. The DMF solution with perovskite precursors was generally used for the LSLX process and the exchanged CQDs are finally concentrated into BTA. After depositing CQD ink on the substrate, the perovskite passivated CQD film was obtained by the subsequent annealing process. Yang et al. (2015) used $MAPbI_3$ perovskite as a passivating agent of CQDs that the coherent lattice matching of $MAPbI_3$ perovskite enhanced the passivation effect and effectively suppressed the aggregation of CQDs. Zhang et al. (2018a, 2018b, 2018c) epitaxially grew inorganic perovskite $CsPbI_3$ layer on the CQD surface, which could provide better passivation of CQDs, thereby reducing charge recombination caused by the trap states (Figure 6D). The PCE of CQDSCs finally reached 10.5% and maintained high long-term light stability. Recently, Albaladejo-Siguan et al. (2020) used three cations $Cs_{0.05}(MA_{0.17}FA_{0.83})_{0.95}Pb(I_{0.9}Br_{0.1})_3$ perovskite for the surface passivation of CQDs. In addition to increasing the CQD coupling, this work demonstrated that the favorable band alignment between the three-cation perovskite and CQDs allowed the charge to be effectively confined within CQDs, inhibiting charge recombination and without hindering the charge transport. The epitaxial growth and complete coating of perovskite show great potential for CQD passivation and thus improve device

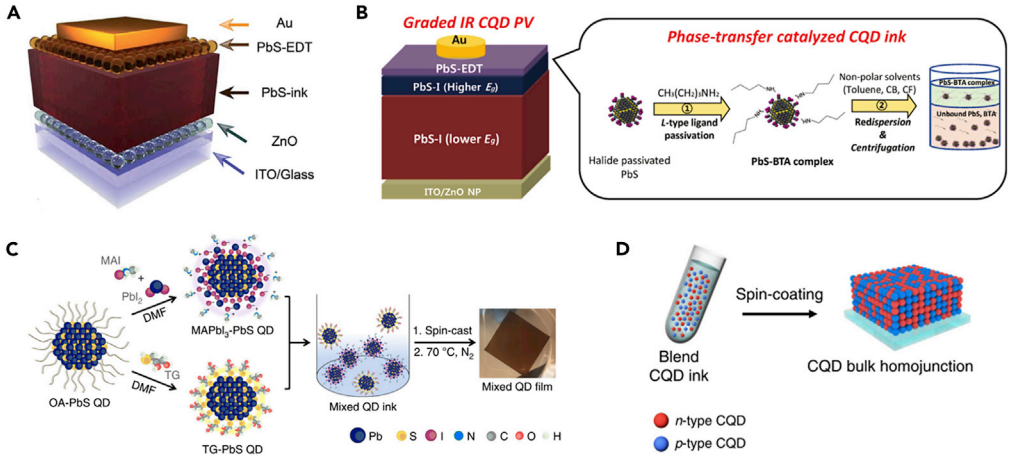

Figure 7. Single Junction of CQDSCs

(A) Schematic diagram of the CQDSCs. Adapted with permission from Gu et al. (2019). Copyright (2019) The Royal Society of Chemistry.

(B) Schematic illustration of device architecture for graded CQDSCs and solvent engineering process of the halide passivated CQDs in nonpolar solvents. Adapted with permission from Kim et al. (2018a, 2018b). Copyright (2018) WILEY-VCH Verlag GmbH & Co. KGaA, Weinheim.

(C) Schematic of the LSLX process of both n-type and p-type CQDs. Adapted with permission from Yang et al. (2017). Copyright (2017) Springer Nature.

(D) Blended CQD inks comprising n-type and p-type CQDs for the fabrication of CQD bulk homojunction films. Adapted with permission from Choi et al. (2020a, 2020b). Copyright (2020) Springer Nature.

photovoltaic performance, which makes perovskite passivation as one of the important directions in current research. Currently, the highest efficiency of PbS CQDSCs came from perovskite passivation. By epitaxially growing a monolayer of $FAPbBr_xI_{3-x}$ perovskite on the CQD surface, the surface defect passivation and packing density of CQD solids were improved and the highest PCE of 13.8% is obtained (Sun et al., 2020).

Therefore, ligand engineering and additive engineering of CQD inks could contribute to the surface chemistry of CQDs. The main aim of the surface chemistry modification is to improve the surface passivation of CQDs, which is to thoroughly remove OA and -OH groups on the CQD surface. The reduction of long alkyl ligands was beneficial to the increase of the packing density of CQD solid films, which could enhance the CQD coupling and charge carrier hopping between dots. The -OH group was the main source of surface defects, and its removal could reduce the sub-bandgap trap states, thereby reducing the recombination of charge carriers, improving carrier mobility, diffusion length, and lifetime of charge carriers. However, compared with other photovoltaic materials, the trap density of CQDs was much higher. Although considerable progress has been made, surface defect passivation of CQDs was still the priority for photovoltaic applications in the future.

Infrared CQDSCs

Single Junction CQDSCs

With the advances to efficiently enhance the charge carrier extraction in CQDSCs, the device structure has undergone a series of evolution, including Schottky junctions (Johnston et al., 2008), p-n heterojunctions (Azmi et al., 2017), and CQD sensitized solar cells (Chen et al., 2017). With respect to the CQD inks, the heterojunction CQDSC with an n-i-p device structure was widely used and obtained a high PCE. The general structure of such a device is composed of ITO/ZnO/CQD-PbX_2 (X = I and Br, prepared from CQD inks)/CQD-EDT/Au, where ZnO is used as an electron transport layer (ETL), CQD-PbX_2 prepared using CQD inks is applied as a photoactive layer and CQD-EDT works as a hole transport layer (HTL), as shown in Figure 7A. It is worthy to note that the development of CQD inks promoted the further optimization of device architecture of CQDSCs and thus further improved device performance.

The studies of CQD inks promoted the realization of graded architecture in the CQDSCs. In the conventional CQDSCs, two depletion regions are formed near the ZnO/CQD-PbX_2 and CQD-PbX_2/CQD-EDT

interfaces, respectively, whereas a quasi-neutral region is formed between these two depletion regions. The built-in electric field in the depletion region facilitates charge carrier extraction, whereas the extraction of photoinduced charge carriers in the quasi-neutral region relies on diffusion. The charge carrier extraction through diffusion generally competes with the charge recombination induced by the sub-bandgap traps due to imperfect surface defect passivation of CQDs. Therefore, the charge recombination in the quasi-neutral region greatly limits the photovoltaic performance of CQDSCs. The CQDSCs with a graded structure can be realized by stacking the CQDs with different sizes in a device, which is beneficial for the band alignment within the device. Meanwhile, the graded architecture also enhances the built-in electric field of the back junction and reduces charge recombination in the quasi-neutral region. However, the commonly used polar solvent BTA dispersed and destroyed the underlying CQD solid films as deposition of multi CQD solid layers (Kim et al., 2018a, 2018b). By forming the PbS-BTA complex on the surface of CQDs could dissolve the CQDs in the non-polar solvents, such as toluene, chlorobenzene, and chloroform, as shown in Figure 7B (Kim et al., 2018a, 2018b). The acquisition of non-polar CQD inks provides the possibility to construct the graded architecture, allowing further optimization of the device structure.

In the conventional CQDSC devices, the p-type CQD-EDT layer that acted as an HTL was usually prepared using the SSLX method, which may offer a chance to further optimize the device architecture and thus boost device performance. Yang et al. (2017) prepared the n-type CQD inks with the $MAPbI_3$ passivation layer on the CQDs, which was combined with p-type CQD inks with 1-thioglycerol (TG) passivating the CQD surface to realize the CQDSCs (Figure 7C). It is notable that the CQDs maintained their unique chemical properties when they were mixed in the solution phase and formed the final CQD solid films. The mixture of donor CQDs and acceptor CQDs could efficiently separate electrons and holes in the CQD solid films, and thereby significantly diminished charge recombination. The efficiency of such hybrid CQDSCs reached 10.4% that was slightly lower than that of conventional heterojunction devices, which was likely due to inferior surface passivation of CQDs. Recently, Choi et al. (2020a, 2020b) adopted a cascade surface modification method to improve the surface passivation of p-type CQDs in the ink system and successfully realized a high-efficiency homojunction device (Figure 7D). The steric hindrance of the p-type ligands prevented full surface coverage. Effective surface passivation of CQDs suppressed the trap-state-induced charge recombination and aggregation of mixed CQD inks. As a result, the carrier diffusion length within the CQD solids was largely increased, and the different physical paths within the CQD solid film significantly improved the separation and transport of photoexcited carriers, thus increasing the thickness of the photoactive layer in the device. The resulting PCE of such a CQDSC gave a PCE of up to 13.3%.

It can be seen that, with the development of the CQD inks, the device structure of CQDSCs can be further optimized to improve device performance. The device structure significantly affected the charge carrier transport and extraction in the solar cells. Currently, the device architecture of efficient CQDSCs was still dominated by the n-i-p heterojunction, which achieved an efficiency of up to 13.8% (Sun et al., 2020). Choi et al. (2020a, 2020b) reported that the homojunction structure was also beneficial to the separation and transmission of carriers, and finally an efficiency of more than 13% was achieved. Thus, the development of homojunction CQDSCs provides a new avenue to further improve device photovoltaic performance.

Tandem Solar Cells

The tunability of infrared E_g in CQDs makes PbS CQDs not only be used for the construction of single-junction infrared solar cells but also fabricated tandem solar cells with other photovoltaic materials. Multi-junction solar cells with appropriate E_g could improve the utilization of the solar spectrum and suppress energy loss in the single-junction solar cells (heating of high-energy photons and transmission of low-energy photons), which provides a strategy to achieve a PCE over single-junction solar cells. Theoretically, the tandem solar cells fabricated with the photovoltaic materials with E_g of 1.75 and 0.9 eV could achieve a PCE of more than 45% (Manekkathodi et al., 2019). For instance, the metal halide perovskites are very promising solution-processed photovoltaic materials and the perovskite solar cells had a high PCE of over 25%. However, although perovskite possessed extraordinary utilization of visible light, the efficiency of capturing infrared photons was still low. In contrast, the PbS CQD has strong light absorption and adjustable E_g in the infrared region, and the low-temperature solution-processable CQD inks could promote the development of tandem solar cells through the combination of low E_g CQDs with high E_g photovoltaic materials.

Zhang et al. (2018a, 2018b, 2018c) used $MAPbI_3$ perovskite and CQDs to make the CQDs/perovskite tandem solar cells and a PCE of 11.03% was achieved. Even though the efficiency of the tandem solar cells was

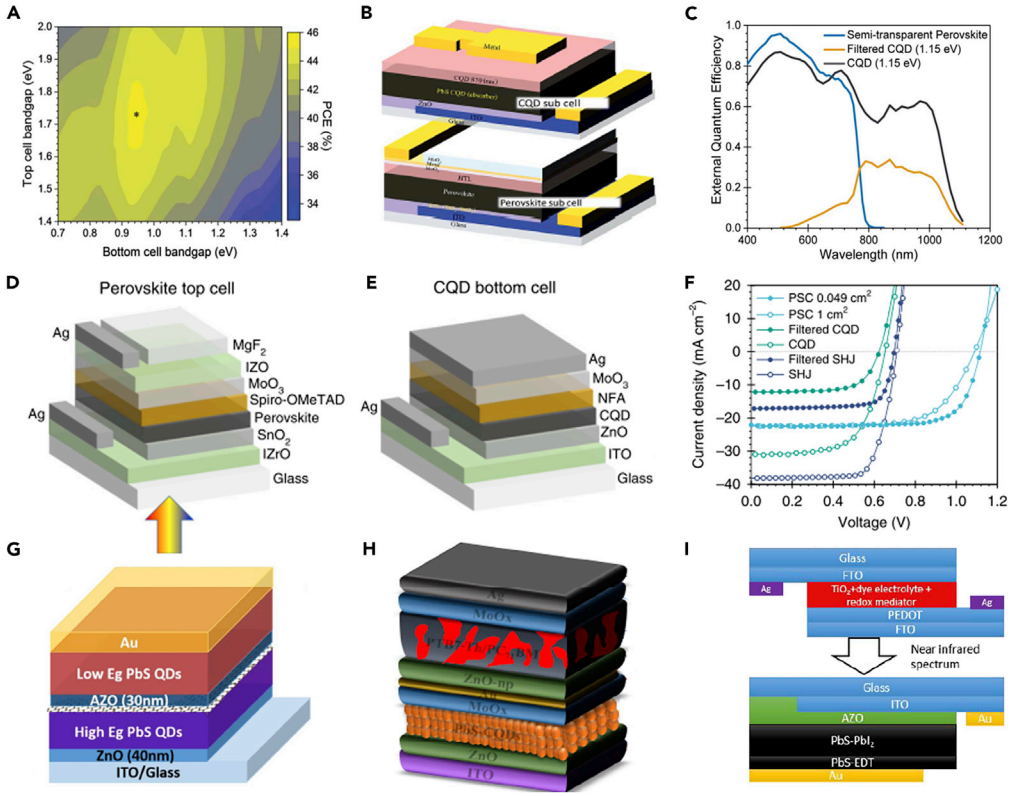

Figure 8. Tandem Infrared Solar Cells

(A) Calculated PCE detailed-balance limit for the hybrid 4T tandem solar cell as a function of the E_g of front cell and back cell.

(B) Schematic of a 4T device.

(C) EQE spectra measured from the front perovskite cell and back CQDSC. Adapted with permission from Manekkathodi et al. (2019). Copyright (2019) The Royal Society of Chemistry.

(D) Device structures of the top perovskite cell.

(E) Device structures of the bottom CQDSC.

(F) *J-V* curves of the top perovskite cell and CQD:organic hybrid bottom cell in the 4T tandem configuration. Adapted with permission from Chen et al. (2020). Copyright (2020) Springer Nature.

(G) Schematic structure of the CQDs/CQDs tandem solar cells. Adapted with permission from Bi et al. (2018a, 2018b). Copyright (2018) American Chemical Society.

(H) Device architecture of CQDs/OPV hybrid tandem photovoltaic devices. Adapted with permission from Aqoma et al. (2017a, 2017b). Copyright (2017) Elsevier Ltd.

(I) Schematic of the four-terminal tandem structure based on the DSSC and CQDSCs. Adapted with permission from Yuan et al. (2020). Copyright (2020) American Chemical Society.

still lower than that of single-junction perovskite solar cells and CQDSCs, the spectrum of the tandem device could be broadened. Figure 8A (Manekkathodi et al., 2019) applied $Cs_{0.05}MA_{0.10}FA_{0.85}PbI_{0.85}Br_{0.15}$ perovskite solar cell as the front cell and the CQDSC fabricated using CQD inks as the back cell to construct a four-terminal (4T) tandem device (Figure 8B). The dielectric-metal-dielectric electrode was used in semi-transparent perovskite front cells, which was composed of MoO_3 (5 nm)/Au (1 nm)/Ag (5 nm)/MoO_3 (35 nm). Based on the low reflectance of incoming light with such an electrode, infrared transmittance was significantly improved. External quantum efficiency (EQE) results of the tandem solar cells indicated that a high EQE value at the CQD exciton peak was gained, which suggests that the CQDSC used as a subcell has a high charge collection efficiency in the infrared range (Figure 8C). Therefore, the back CQDSCs and front perovskite cells exhibited good complementary utilization of the solar spectrum. Finally, the PCE of the tandem solar cell reached 20.2%, exceeding 18% for the single-junction perovskite solar cells. Chen et al. (2020) increased the optical path length and electron diffusion length through boosting the solvent extraction techniques, and thereby further increasing the PCE of $Cs_{0.05}FA_{0.81}MA_{0.14}PbI_{2.55}Br_{0.45}$ perovskite top cell to ~19% (Figure 8D). In terms of the bottom cell, the CQDs:organic hybrid structure was applied to

supplement the inherent absorption defects of CQDs near the exciton valleys (Figure 8E). Therefore, the filtered CQD bottom cell provided an additional 5% efficiency for the perovskite top cell, making the 4T tandem devices reach a PCE of 24.4% (Figure 8F).

Therefore, the infrared E_g of CQDs provides the possibility to improve the utilization of the solar spectrum. Since perovskite shows excellent absorption in the visible region and impressive PCEs, the tandem solar cells of CQDs and perovskite have become an important way to further improve the device photovoltaic performance. Moreover, with the development of CQDs and perovskites, the PCE of tandem solar cells has exceeded 24% (Chen et al., 2020). The CQD inks have promoted the development of high-efficiency and low-cost solution processing tandem solar cells, which could make full use of the infrared absorption characteristics of CQDs and ultimately realize the complementarity between different photovoltaic materials.

Additionally, the CQDs can also be combined with CQDs (CQDs/CQDs), organic photovoltaic materials (CQDs/OPV), and dye-sensitized solar cells (CQDs/DSSC) to construct efficient tandem solar cells. For CQDs/CQDs tandem solar cells, the CQDs with different E_g have complementary light absorption characteristics and well-matched current (Figure 8G). Biet al. (2018a, 2018b) used graphene as an intermediate layer to reduce optical and electronic losses in the CQDs/CQDs tandem solar cells. Shi et al. (2017) improved each part of intermediate recombination layers, where low-temperature co-solvent treatment of ZnO and hole selectivity of PbS-EDT ensured that the sub-cells were not damaged and the electrons were blocked. The PEDOT intermediate layer and Au intermediate layer could provide large-scale production of tandem devices and improve device lifetime and performance. As a result, the PCE of CQDs/CQDs tandem solar cells exceeded 8%. For PbS/OPV tandem solar cells, the PTB7:PCBM was used as photoactive materials for sub-cells (Figure 8H). Amassian group conducted a series of explorations on the intermediate layer of CQDs/OPV tandem solar cells. The interlayer structure of MoO_x/Au/AZO (Aqoma et al., 2017a, 2017b) was demonstrated to have an excellent charge recombination effect, in which the island-shaped Au reduced series resistance and increased shunt resistance (Kim et al., 2017). Furthermore, the sputtered dense AZO could protect the organic front cell from being penetrated by the CQD inks, and the CQDs with a low E_g were used for back cell fabrication (Kim et al., 2018a, 2018b). Kim et al. improved the recombination properties of the intermediate layer by using MoOx/ZnO/poly[(9,9-bis(30-(N,N-dimethylamino)propyl)-2,7-fluorene)-alt-2,7-(9,9-dioctylfluorene)] (PFN), in which the PFN could increase the built-in potential and reduced the contact resistance in the tandem devices (Kim et al., 2015). Recently, CQDs/DSSC tandem solar cells have also been developed and achieved a PCE of more than 12% (Yuan et al., 2020), which was derived from the adjustment of dye and E_g of CQDs (Figure 8I).

It can be seen that matched photocurrent and complementary light absorption are the basis for the construction of a tandem solar cell. Several studies have proved that the interlayer within the tandem solar cells is crucial to improve device performance. Among various tandem solar cells, the efficiency of CQDs/CQDs, CQDs/OPV, and CQDs/DSSC tandem solar cells was less than 13%, whereas the efficiency of CQDs/perovskite tandem solar cells reached 24.4%, which was still less than the highest efficiency of perovskite solar cells. Therefore, looking for photovoltaic materials with better matching photocurrent and making full use of the infrared absorption characteristics of CQDs is challenging for the tandem solar cells.

However, it is notable that the PbS CQDs are toxic photovoltaic materials. The $(TMS)_2S$ used as a sulfur source during the synthesis of CQDs possesses a strong pungent odor, which may cause not only air pollution but also obvious discomfort to the human physiological system. Lead compounds can damage the human nervous system and digestive system. If the PbS CQD is handled improperly, it will endanger human health and result in environmental pollution, which may hinder the commercialization of PbS CQDSCs.

CONCLUSION AND OUTLOOK

In summary, the solution-processed CQDs have emerged as a high-potential candidate for infrared solar cells, and remarkable progress has been obtained in the CQDSCs with an efficiency of over 13% being achieved. To improve the usage of solar energy, the light absorbers with an ability to harvest the infrared photons were critical for broadening the light absorption of solar cells. By controlling the size of CQDs the E_g of CQDs can be well tuned in the infrared region, which is of great importance for the construction of infrared single-junction and/or tandem solar cells to further boost device efficiency. Combined with the CQD inks the solution-processed fabrication method provided a feasible strategy to scalably produce infrared solar cells using roll-to-roll blade-coating or spray-coating approaches. Meanwhile, the surface

ligands of CQDs can be more thoroughly replaced using the CQD ink technologies, and thus the improved surface defect passivation of CQDs could be obtained through the solvent engineering of the inks and the surface modification of CQDs. To increase the usage of solar energy, construction of the tandem devices by combining the infrared CQDSCs with the other visible solar cells, such as perovskite solar cells, organic solar cells, or dye-sensitized solar cells, could provide a potential avenue.

Even though remarkable progress has been obtained for the photovoltaic performance and device stability of the infrared CQDSCs, the device efficiency was still much lower than that of the theoretical PCEs, as well as other infrared solar cells, such as silicon solar cells and bulk perovskite solar cells. Therefore, more fundamental studies may be needed to be carried out to further improve the device performance of the infrared CQDSCs. We here present the possible issues or challenges for the further development of infrared solar cells with the CQD ink technologies.

(I) The CQD ink provides a feasible strategy to thoroughly remove the long-chain organic ligands and effectively passivate the surface defects of CQDs, but compared with other infrared light absorbers, such as silicon, the trap density in the CQD solid films is still too high, which significantly affects the charge carrier extraction and thus the device photovoltaic performance. Thus, during the ligand exchange of CQDs for the preparation of CQD inks, fine controlling the surface chemistry of CQDs is significantly required by controlling the solvent, ligands, and/or operation process to improve the surface defect passivation of CQDs. Meanwhile, to efficiently passivate the CQD surface using molecule engineering, more surface passivation materials or methods may need to be studied, such as epitaxial growth inorganic perovskite or other inorganic passivation layers, to promote the surface passivation of CQDs to a new level.

(II) Most of the highly efficient infrared CQDSCs were prepared using the spin-coating method combined with the CQD inks in the laboratory conditions, which could prepare the high-quality CQD solid films. The continuous solution-processed roll-to-roll processing, such as spray-coating or printing-coating, offers a potential method for the scalable production of CQDSCs. However, the optoelectronic properties of the CQD solid films are largely affected by the deposition operation and there are still few works on depositing CQD solid films with novel large-scale preparation methods. More theoretical or experimental studies on the deposition methods of CQD solid films would provide insight into the physical and chemical properties of CQDs and thus obtain the large-sized CQDSC panels toward future commercialization.

(III) So far, the state-of-the-art infrared CQDSCs were generally fabricated using PbS CQDs as a light absorber, which may face the toxicity issues for further practical applications. The no toxic or less toxic infrared CQD inks may need to be explored, such as Ag_2S, Ag_2S, $CuInS_2$, or $AgBiS_2$ CQD inks, for environment-friendly infrared CQDSCs. The $AgBiS_2$ CQDSCs yielded a PCE of 6.3% (Bernechea et al., 2016), showing potential for low-toxic CQDSCs. However, the CQD inks prepared with these CQDs may be significantly different from the PbS CQD inks owing to the complex surface chemistry of CQDs and the ink system. We believe that, with more efforts taking on the ligand exchange of these CQDs and the related CQD ink system, it is still possible to prepare the no toxic CQD inks and therefore obtain the no toxic devices, showing comparable or higher efficiency than that of PbS CQD-based devices.

Overall, the CQD inks are very promising for the next-generation infrared solar cells by taking advantage of the unique properties of infrared CQDs. We believe that, with further breakthroughs in the surface chemistry of CQDs and the preparation technologies of CQD sold films, the infrared CQDSCs with higher efficiency and stability will be achieved in the near future.

ACKNOWLEDGMENTS

This work was supported by the National Natural Science Foundation of China (Grant No. 51872014), the Recruitment Program of Global Experts, Fundamental Research Funds for the Central Universities, the "111" project (B17002), and the Swedish Energy Agency.

AUTHOR CONTRIBUTIONS

S.Z. and J.C. wrote the manuscript and prepared the figures. X.Z. and E.M.J.J. provided an outline and guided writing. All authors read and discussed the manuscript.

REFERENCES

Albaladejo-Siguan, M., Becker-Koch, D., Taylor, A.D., Sun, Q., Lami, V., Oppenheimer, P.G., Paulus, F., and Vaynzof, Y. (2020). Efficient and stable PbS quantum dot solar cells by triple-cation perovskite passivation. ACS Nano *14*, 384–393.

Aqoma, H., and Jang, S.-Y. (2018). Solid-state-ligand-exchange free quantum dot ink-based solar cells with an efficiency of 10.9%. Energy Environ. Sci. *11*, 1603–1609.

Aqoma, H., Al Mubarok, M., Hadmojo, W.T., Lee, E.H., Kim, T.W., Ahn, T.K., Oh, S.H., and Jang, S.Y. (2017a). High-efficiency photovoltaic devices using trap-controlled quantum-dot ink prepared via phase-transfer exchange. Adv. Mater. *29*, 1605756.

Aqoma, H., Azmi, R., Oh, S.-H., and Jang, S.-Y. (2017b). Solution-processed colloidal quantum dot/organic hybrid tandem photovoltaic devices with 8.3% efficiency. Nano Energy *31*, 403–409.

Azmi, R., Sinaga, S., Aqoma, H., Seo, G., Ahn, T.K., Park, M., Ju, S.-Y., Lee, J.-W., Kim, T.-W., Oh, S.-H., and Jang, S.-Y. (2017). Highly efficient air-stable colloidal quantum dot solar cells by improved surface trap passivation. Nano Energy *39*, 86–94.

Bernechea, M., Miller, N.C., Xercavins, G., So, D., Stavrinadis, A., and Konstantatos, G. (2016). Solution-processed solar cells based on environmentally friendly $AgBiS_2$ nanocrystals. Nat. Photon. *10*, 521–525.

Bi, Y., Pradhan, S., Gupta, S., Akgul, M.Z., Stavrinadis, A., and Konstantatos, G. (2018a). Infrared solution-processed quantum dot solar cells reaching external quantum efficiency of 80% at 1.35 μm and J_{sc} in excess of 34 mA cm^{-2}. Adv. Mater. *30*, 1704928.

Bi, Y., Pradhan, S., Akgul, M.Z., Gupta, S., Stavrinadis, A., Wang, J., and Konstantatos, G. (2018b). Colloidal quantum dot tandem solar cells using chemical vapor deposited graphene as an atomically thin intermediate recombination layer. ACS Energy Lett. *3*, 1753–1759.

Cademartiri, L., Montanari, E., Calestani, G., Migliori, A., Guagliardi, A., and Ozin, G.A. (2006). Size-dependent extinction coefficients of PbS quantum dots. J. Am. Chem. Soc. *128*, 10337–10346.

Chan, S., Liu, M., Latham, K., Haruta, M., Kurata, H., Teranishi, T., and Tachibana, Y. (2017). Monodisperse and size-tunable PbS colloidal quantum dots via heterogeneous precursors. J. Mater. Chem. C *5*, 2182–2187.

Chen, J., Shi, C., Zhang, Z., Xiao, G., Shao, Z., and Li, N. (2017). All-solid-state compact PbS quantum dot film sensitized TiO_2 nanorod array solar cell with 4.81% photoelectric conversion efficiency. Acta Phys. Chim. Sin. *33*, 2029–2034.

Chen, B., Baek, S.W., Hou, Y., Aydin, E., De Bastiani, M., Scheffel, B., Proppe, A., Huang, Z., Wei, M., Wang, Y.K., et al. (2020). Enhanced optical path and electron diffusion length enable high-efficiency perovskite tandems. Nat. Commun. *11*, 1257.

Choi, M.J., Kim, Y., Lim, H., Alarousu, E., Adhikari, A., Shaheen, B.S., Kim, Y.H., Mohammed, O.F., Sargent, E.H., Kim, J.Y., and Jung, Y.S. (2019). Tuning solute-redistribution dynamics for scalable fabrication of colloidal quantum-dot optoelectronics. Adv. Mater. *31*, e1805886.

Choi, M.J., Garcia de Arquer, F.P., Proppe, A.H., Seifitokaldani, A., Choi, J., Kim, J., Baek, S.W., Liu, M., Sun, B., Biondi, M., et al. (2020a). Cascade surface modification of colloidal quantum dot inks enables efficient bulk homojunction photovoltaics. Nat. Commun. *11*, 103.

Choi, J., Choi, M.J., Kim, J., Dinic, F., Todorovic, P., Sun, B., Wei, M., Baek, S.W., Hoogland, S., Garcia de Arquer, F.P., et al. (2020b). Stabilizing surface passivation enables stable operation of colloidal quantum dot photovoltaic devices at maximum power point in an air ambient. Adv. Mater. *32*, e1906497.

Fan, J.Z., Andersen, N.T., Biondi, M., Todorovic, P., Sun, B., Ouellette, O., Abed, J., Sagar, L.K., Choi, M.J., Hoogland, S., et al. (2019). Mixed lead halide passivation of quantum dots. Adv. Mater. *31*, e1904304.

Fischer, A., Rollny, L., Pan, J., Carey, G.H., Thon, S.M., Hoogland, S., Voznyy, O., Zhitomirsky, D., Kim, J.Y., Bakr, O.M., and Sargent, E.H. (2013). Directly deposited quantum dot solids using a colloidally stable nanoparticle ink. Adv. Mater. *25*, 5742–5749.

Gu, M., Wang, Y., Yang, F., Lu, K., Xue, Y., Wu, T., Fang, H., Zhou, S., Zhang, Y., Ling, X., et al. (2019). Stable PbS quantum dot ink for efficient solar cells by solution-phase ligand engineering. J. Mater. Chem. A *7*, 15951–15959.

Han, B. (2020). Near-infrared quantum dots: small particles, large energy. Acta Phys. Chim. Sin. *36*, 1911025–1911030.

Hines, M.A., and Scholes, G.D. (2003). Colloidal PbS nanocrystals with size-tunable near-infrared emission: observation of post-synthesis self-narrowing of the particle size distribution. Adv. Mater. *15*, 1844–1849.

Hou, B., Cho, Y., Kim, B.S., Hong, J., Park, J.B., Ahn, S.J., Sohn, J.I., Cha, S., and Kim, J.M. (2016). Highly monodispersed PbS quantum dots for outstanding cascaded-junction solar cells. ACS Energy Lett. *1*, 834–839.

Huang, P.-C., Yang, W.-C., and Lee, M.-W. (2013). $AgBiS_2$ semiconductor-sensitized solar cells. J. Phys. Chem. C *117*, 18308–18314.

Hwang, I., Seol, M., Kim, H., and Yong, K. (2013). Improvement of photocurrent generation of Ag_2S sensitized solar cell through co-sensitization with CdS. Appl. Phys. Lett. *103*, 023902.

Jang, J., Shim, H.C., Ju, Y., Song, J.H., An, H., Yu, J.S., Kwak, S.W., Lee, T.M., Kim, I., and Jeong, S. (2015). All-solution-processed PbS quantum dot solar modules. Nanoscale *7*, 8829–8834.

Jia, D., Chen, J., Zheng, S., Phuyal, D., Yu, M., Tian, L., Liu, J., Karis, O., Rensmo, H., Johansson, E.M.J., and Zhang, X. (2019). Highly stabilized quantum dot ink for efficient infrared light absorbing solar cells. Adv. Energy Mater. *9*, 1902809.

Jo, J.W., Kim, Y., Choi, J., de Arquer, F.P.G., Walters, G., Sun, B., Ouellette, O., Kim, J., Proppe, A.H., Quintero-Bermudez, R., et al. (2017). Enhanced open-circuit voltage in colloidal quantum dot photovoltaics via reactivity-controlled solution-phase ligand exchange. Adv. Mater. *29*, 1703627.

Jo, J.W., Choi, J., Garcia de Arquer, F.P., Seifitokaldani, A., Sun, B., Kim, Y., Ahn, H., Fan, J., Quintero-Bermudez, R., Kim, J., et al. (2018). Acid-assisted ligand exchange enhances coupling in colloidal quantum dot solids. Nano Lett. *18*, 4417–4423.

Johnston, K.W., Pattantyus-Abraham, A.G., Clifford, J.P., Myrskog, S.H., MacNeil, D.D., Levina, L., and Sargent, E.H. (2008). Schottky-quantum dot photovoltaics for efficient infrared power conversion. Appl. Phys. Lett. *92*, 151115.

Kagan, C.R., Lifshitz, E., Sargent, E.H., and Talapin, D.V. (2016). Building devices from colloidal quantum dots. Science *353*, 885.

Kiani, A., Sutherland, B.R., Kim, Y., Ouellette, O., Levina, L., Walters, G., Dinh, C.-T., Liu, M., Voznyy, O., Lan, X., et al. (2016). Single-step colloidal quantum dot films for infrared solar harvesting. Appl. Phys. Lett. *109*, 183105.

Kim, T., Gao, Y., Hu, H., Yan, B., Ning, Z., Jagadamma, L.K., Zhao, K., Kirmani, A.R., Eid, J., Adachi, M.M., et al. (2015). Hybrid tandem solar cells with depleted-heterojunction quantum dot and polymer bulk heterojunction subcells. Nano Energy *17*, 196–205.

Kim, T., Palmiano, E., Liang, R.Z., Hu, H., Murali, B., Kirmani, A.R., Firdaus, Y., Gao, Y., Sheikh, A., Yuan, M., et al. (2017). Hybrid tandem quantum dot/organic photovoltaic cells with complementary near infrared absorption. Appl. Phys. Lett. *110*, 223903.

Kim, J., Ouellette, O., Voznyy, O., Wei, M., Choi, J., Choi, M.J., Jo, J.W., Baek, S.W., Fan, J., Saidaminov, M.I., et al. (2018a). Butylamine-catalyzed synthesis of nanocrystal inks enables efficient infrared CQD solar cells. Adv. Mater. *30*, e1803830.

Kim, T., Firdaus, Y., Kirmani, A.R., Liang, R.-Z., Hu, H., Liu, M., El Labban, A., Hoogland, S., Beaujuge, P.M., Sargent, E.H., and Amassian, A. (2018b). Hybrid tandem quantum dot/organic solar cells with enhanced photocurrent and efficiency via ink and interlayer engineering. ACS Energy Lett. *3*, 1307–1314.

Kim, Y., Che, F., Jo, J.W., Choi, J., Garcia de Arquer, F.P., Voznyy, O., Sun, B., Kim, J., Choi, M.J., Quintero-Bermudez, R., et al. (2019). A facet-specific quantum dot passivation strategy for colloid management and efficient infrared photovoltaics. Adv. Mater. *31*, e1805580.

Kirmani, A.R., Sheikh, A.D., Niazi, M.R., Haque, M.A., Liu, M., de Arquer, F.P.G., Xu, J., Sun, B., Voznyy, O., Gasparini, N., et al. (2018). Overcoming the ambient manufacturability-scalability-performance bottleneck in colloidal quantum dot photovoltaics. Adv. Mater. *30*, e1801661.

Kramer, I.J., Moreno-Bautista, G., Minor, J.C., Kopilovic, D., and Sargent, E.H. (2014). Colloidal

quantum dot solar cells on curved and flexible substrates. Appl. Phys. Lett. *105*, 163902.

Kramer, I.J., Minor, J.C., Moreno-Bautista, G., Rollny, L., Kanjanaboos, P., Kopilovic, D., Thon, S.M., Carey, G.H., Chou, K.W., Zhitomirsky, D., et al. (2015). Efficient spray-coated colloidal quantum dot solar cells. Adv. Mater. *27*, 116–121.

Liu, M., Voznyy, O., Sabatini, R., Garcia de Arquer, F.P., Munir, R., Balawi, A.H., Lan, X., Fan, F., Walters, G., Kirmani, A.R., et al. (2017). Hybrid organic-inorganic inks flatten the energy landscape in colloidal quantum dot solids. Nat. Mater. *16*, 258–263.

Liu, M., Che, F., Sun, B., Voznyy, O., Proppe, A., Munir, R., Wei, M., Quintero-Bermudez, R., Hu, L., Hoogland, S., et al. (2019a). Controlled steric hindrance enables efficient ligand exchange for stable, infrared-bandgap quantum dot inks. ACS Energy Lett. *4*, 1225–1230.

Liu, M., Chen, Y., Tan, C.S., Quintero-Bermudez, R., Proppe, A.H., Munir, R., Tan, H., Voznyy, O., Scheffel, B., Walters, G., et al. (2019b). Lattice anchoring stabilizes solution-processed semiconductors. Nature *570*, 96–101.

Lu, K., Wang, Y., Liu, Z., Han, L., Shi, G., Fang, H., Chen, J., Ye, X., Chen, S., Yang, F., et al. (2018). High-efficiency PbS quantum-dot solar cells with greatly simplified fabrication processing via "solvent-curing". Adv. Mater. *30*, e1707572.

Lu, H., Carroll, G.M., Neale, N.R., and Beard, M.C. (2019). Infrared quantum dots: progress, challenges, and opportunities. ACS Nano *13*, 939–953.

Luther, J.M., Gao, J., Lloyd, M.T., Semonin, O.E., Beard, M.C., and Nozik, A.J. (2010). Stability assessment on a 3% bilayer PbS/ZnO quantum dot heterojunction solar cell. Adv. Mater. *22*, 3704–3707.

Manekkathodi, A., Chen, B., Kim, J., Baek, S.-W., Scheffel, B., Hou, Y., Ouellette, O., Saidaminov, M.I., Voznyy, O., Madhavan, V.E., et al. (2019). Solution-processed perovskite-colloidal quantum dot tandem solar cells for photon collection beyond 1000 nm. J. Mater. Chem. A *7*, 26020–26028.

Moreels, I., Lambert, K., Smeets, D., De Muynck, D., Nollet, T., Martins, J.C., Vanhaecke, F., Vantomme, A., Delerue, C., Allan, G., and Hens, Z. (2009). Size-dependent optical properties of colloidal PbS quantum dots. ACS Nano *3*, 3023–3030.

Ning, Z., Dong, H., Zhang, Q., Voznyy, O., and Sargent, E.H. (2014). Solar cells based on inks of n-type colloidal quantum dots. ACS Nano *8*, 10321–10327.

Peer, A., Hu, Z., Singh, A., Hollingsworth, J.A., Biswas, R., and Htoon, H. (2017). Photoluminescence enhancement of $CuInS_2$ quantum dots in solution coupled to plasmonic gold nanocup array. Small *13*, 1700660.

Polman, A., Knight, M., Garnett, E.C., Ehrler, B., and Sinke, W.C. (2016). Photovoltaic materials: present efficiencies and future challenges. Science *352*, aad4424.

Sargent, E.H. (2012). Colloidal quantum dot solar cells. Nat. Photon. *6*, 133–135.

Semonin, O.E., Luther, J.M., Choi, S., Chen, H.Y., Gao, J.B., Nozik, A.J., and Beard, M.C. (2011). Peak external photocurrent quantum efficiency exceeding 100% via MEG in a quantum dot solar cell. Science *334*, 1530–1533.

Shi, G., Wang, Y., Liu, Z., Han, L., Liu, J., Wang, Y., Lu, K., Chen, S., Ling, X., Li, Y., et al. (2017). Stable and highly efficient PbS quantum dot tandem solar cells employing a rationally designed recombination layer. Adv. Energy Mater. *7*, 1602667.

Shockley, W., and Queisser, H.J. (1961). Detailed balance limit of efficiency of p-n junction solar cells. J. Appl. Phys. *32*, 510–519.

Sliz, R., Lejay, M., Fan, J.Z., Choi, M.J., Kinge, S., Hoogland, S., Fabritius, T., Garcia de Arquer, F.P., and Sargent, E.H. (2019). Stable colloidal quantum dot inks enable inkjet-printed high-sensitivity infrared photodetectors. ACS Nano *13*, 11988–11995.

Spangler, L.C., Lu, L., Kiely, C.J., Berger, B.W., and McIntosh, S. (2016). Biomineralization of PbS and PbS-CdS core-shell nanocrystals and their application in quantum dot sensitized solar cells. J. Mater. Chem. A *4*, 6107–6115.

Stavrinadis, A., Pradhan, S., Papagiorgis, P., Itskos, G., and Konstantatos, G. (2017). Suppressing deep traps in PbS colloidal quantum dots via facile iodide substitutional doping for solar cells with efficiency >10%. ACS Energy Lett. *2*, 739–744.

Sun, B., Voznyy, O., Tan, H., Stadler, P., Liu, M., Walters, G., Proppe, A.H., Liu, M., Fan, J., Zhuang, T., et al. (2017). Pseudohalide-exchanged quantum dot solids achieve record quantum efficiency in infrared photovoltaics. Adv. Mater. *29*, 1700749.

Sun, B., Johnston, A., Xu, C., Wei, M., Huang, Z., Jiang, Z., Zhou, H., Gao, Y., Dong, Y., Ouellette, O., et al. (2020). Monolayer perovskite bridges enable strong quantum dot coupling for efficient solar cells. Joule *4*, 1542–1556.

Tian, Q., Deng, D., Zhang, Z., Li, Y., Yang, Y., and Guo, X. (2017). Facile synthesis of Ag_2Se quantum dots and their application in dye/Ag_2Se co-sensitized solar cells. J. Mater. Sci. *52*, 12131–12140.

Voznyy, O., Levina, L., Fan, J.Z., Askerka, M., Jain, A., Choi, M.J., Ouellette, O., Todorovic, P., Sagar, L.K., and Sargent, E.H. (2019). Machine learning accelerates discovery of optimal colloidal quantum dot synthesis. ACS Nano *13*, 11122–11128.

Wang, Y., Lu, K., Han, L., Liu, Z., Shi, G., Fang, H., Chen, S., Wu, T., Yang, F., Gu, M., et al. (2018). In situ passivation for efficient PbS quantum dot solar cells by precursor engineering. Adv. Mater. *30*, 1704871.

Wang, Y., Liu, Z., Huo, N., Li, F., Gu, M., Ling, X., Zhang, Y., Lu, K., Han, L., Fang, H., et al. (2019). Room-temperature direct synthesis of semi-conductive PbS nanocrystal inks for optoelectronic applications. Nat. Commun. *10*, 5136.

Xia, Y., Liu, S., Wang, K., Yang, X., Lian, L., Zhang, Z., He, J., Liang, G., Wang, S., Tan, M., et al. (2019). Cation-exchange synthesis of highly monodisperse PbS quantum dots from ZnS nanorods for efficient infrared solar cells. Adv. Funct. Mater. *30*, 1907379.

Xia, Y., Chen, W., Zhang, P., Liu, S., Wang, K., Yang, X., Tang, H., Lian, L., He, J., Liu, X., et al. (2020). Facet control for trap-state suppression in colloidal quantum dot solids. Adv. Funct. Mater. *30*, 2000594.

Xu, J., Voznyy, O., Liu, M., Kirmani, A.R., Walters, G., Munir, R., Abdelsamie, M., Proppe, A.H., Sarkar, A., Garcia de Arquer, F.P., et al. (2018). 2D matrix engineering for homogeneous quantum dot coupling in photovoltaic solids. Nat. Nanotechnol. *13*, 456–462.

Yang, Z., Janmohamed, A., Lan, X., Garcia de Arquer, F.P., Voznyy, O., Yassitepe, E., Kim, G.H., Ning, Z., Gong, X., Comin, R., and Sargent, E.H. (2015). Colloidal quantum dot photovoltaics enhanced by perovskite shelling. Nano Lett. *15*, 7539–7543.

Yang, Z., Fan, J.Z., Proppe, A.H., Arquer, F.P.G., Rossouw, D., Voznyy, O., Lan, X., Liu, M., Walters, G., Quintero-Bermudez, R., et al. (2017). Mixed-quantum-dot solar cells. Nat. Commun. *8*, 1325.

Yuan, L., Michaels, H., Roy, R., Johansson, M., Öberg, V., Andruszkiewicz, A., Zhang, X., Freitag, M., and Johansson, E.M.J. (2020). Four-terminal tandem solar cell with dye-sensitized and PbS colloidal quantum-dot-based subcells. ACS Appl. Energy Mater. *3*, 3157–3161.

Zhang, X., and Johansson, E.M.J. (2016). Utilizing light trapping interference effects in microcavity structured colloidal quantum dot solar cells: a combined theoretical and experimental approach. Nano Energy *28*, 71–77.

Zhang, X., Liu, J., and Johansson, E.M. (2015). Efficient charge-carrier extraction from Ag_2S quantum dots prepared by the silar method for utilization of multiple exciton generation. Nanoscale *7*, 1454–1462.

Zhang, X., Aitola, K., Hagglund, C., Kaskela, A., Johansson, M.B., Sveinbjornsson, K., Kauppinen, E.I., and Johansson, E.M. (2017a). Dry-deposited transparent carbon nanotube film as front electrode in colloidal quantum dot solar cells. Chemsuschem *10*, 434–441.

Zhang, Z., Chen, Z., Zhang, J., Chen, W., Yang, J., Wen, X., Wang, B., Kobamoto, N., Yuan, L., Stride, J.A., et al. (2017b). Significant improvement in the performance of PbSe quantum dot solar cell by introducing a $CsPbBr_3$ perovskite colloidal nanocrystal back layer. Adv. Energy Mater. *7*, 1601773.

Zhang, C., Xia, Y., Zhang, Z., Huang, Z., Lian, L., Miao, X., Zhang, D., Beard, M.C., and Zhang, J. (2017c). Combination of cation exchange and quantized ostwald ripening for controlling size distribution of lead chalcogenide quantum dots. Chem. Mater. *29*, 3615–3622.

Zhang, X., Öberg, V.A., Du, J., Liu, J., and Johansson, E.M.J. (2018a). Extremely lightweight and ultra-flexible infrared light-converting quantum dot solar cells with high power-per-weight output using a solution-processed bending durable silver nanowire-based electrode. Energy Environ. Sci. *11*, 354–364.

Zhang, X., Zhang, J., Phuyal, D., Du, J., Tian, L., Öberg, V.A., Johansson, M.B., Cappel, U.B., Karis, O., Liu, J., et al. (2018b). Inorganic $CsPbI_3$ perovskite coating on PbS quantum dot for highly efficient and stable infrared light converting solar cells. Adv. Energy Mater. *8*, 1702049.

Zhang, Y., Gu, M., Li, N., Xu, Y., Ling, X., Wang, Y., Zhou, S., Li, F., Yang, F., Ji, K., et al. (2018c). Realizing solution-processed monolithic PbS QDs/perovskite tandem solar cells with high UV stability. J. Mater. Chem. A *6*, 24693–24701.

Zhang, X., Cappel, U.B., Jia, D., Zhou, Q., Du, J., Sloboda, T., Svanström, S., Johansson, F.O.L., Lindblad, A., Giangrisostomi, E., et al. (2019). Probing and controlling surface passivation of PbS quantum dot solid for improved performance of infrared absorbing solar cells. Chem. Mater. *31*, 4081–4091.

Zhou, S., Liu, Z., Wang, Y., Lu, K., Yang, F., Gu, M., Xu, Y., Chen, S., Ling, X., Zhang, Y., et al. (2019). Towards scalable synthesis of high-quality PbS colloidal quantum dots for photovoltaic applications. J. Mater. Chem. C *7*, 1575–1583.